Inorg. Chem. **2003**, *42*, 5211–5218

Inorganic Chemistry
Article

Synthesis, Characterization, and Laser Flash Photolysis Reactivity of a Carbonmonoxy Heme Complex

David W. Thompson,[†] Ryan M. Kretzer,[†] Estelle L. Lebeau,[†] Donald V. Scaltrito,[†] Reza A. Ghiladi,[†] Kin-Chung Lam,[‡] Arnold L. Rheingold,[‡] Kenneth D. Karlin,*,[†] and Gerald J. Meyer*,[†]

Department of Chemistry, The Johns Hopkins University, Charles and 34th Streets, Baltimore, Maryland 21218, and Crystallography Laboratory, Department of Chemistry, University of Delaware, Newark, Delaware 19716

Received December 26, 2002

We present here the synthesis, characterization, and flash photolysis study of [(F_8TPP)Fe^{II}(CO)(THF)] (**1**) {F_8TPP $=$ tetrakis(2,6-difluorophenyl)porphyrinate(2–)}. Complex **1** crystallizes from THF/heptane solvent system as a tris-THF solvate, [(F_8TPP)Fe^{II}(CO)(THF)]•3THF (**1•3THF**), with ferrous ion in the porphyrin plane ($C_{61}H_{52}F_8FeN_4O_5$; $a = 11.7908(2)$ Å, $b = 20.4453(2)$ Å, $c = 39.9423(3)$, $\alpha = 90°$, $\beta = 90°$, $\gamma = 90°$; orthorhombic, $P2_12_12_1$, $Z = 8$; Fe–N_4(av) $= 2.00$ Å; N–Fe–N (all) $= 90.0°$). This complex (as **1•THF**) has also been characterized by ^{1}H NMR {six-coordinate, low-spin heme; CD_3CN, RT, δ 8.82 (s, pyrrole-H, 8H), 7.89 (s, *para*-phenyl-H, 8H), 7.46 (s, *meta*-phenyl-H, 4H), 3.58 (s, THF, 8H), 1.73 (s, THF, 8H)}, ^{2}H NMR (pyrrole-deuterated analogue) [(F_8TPP-d_8)Fe^{II}(CO)(THF)] {THF, RT, δ 8.78 ppm (s, pyrrole-D)}, ^{13}C NMR (on ^{13}CO-enriched adduct) {THF-d_8, RT, δ 206.5 ppm; CD_2Cl_2, RT, δ 206.1 ppm}, UV–vis {THF, RT, λ_{max}, 411 (Soret), 525 nm}, and IR {293 K, solution, ν_{CO} 1979 cm^{-1} (THF), 1976 cm^{-1} (acetone), 1982 cm^{-1} (CH_3CN)} spectroscopies. In order to more fully understand the intricacies of solvent–ligand binding (as compared to CO rebinding to the photolyzed heme), we have also synthesized the bis-THF adduct [(F_8TPP)Fe^{II}(THF)$_2$]. Complex **2** also crystallizes from THF/heptane solvent system as a bis-THF solvate, [(F_8TPP)Fe^{II}(THF)$_2$]•2THF (**2•2THF**), with ferrous iron in the porphyrin plane ($C_{60}H_{52}F_8FeN_4O_4$; $a = 21.3216(3)$ Å, $b = 12.1191(2)$ Å, $c = 21.0125(2)$ Å, $\alpha = 90°$, $\beta = 105.3658(5)°$, $\gamma = 90°$; monoclinic, $C2/c$, $Z = 4$; Fe–N_4(av) $= 2.07$ Å; N–Fe–N (all) $= 90.0°$). Further characterization of **2** includes UV–vis {THF, λ_{max}, 421 (Soret), 542 nm} and ^{1}H NMR {six-coordinate, high spin heme; THF-d_8, RT, δ 56.7 (s, pyrrole-H, 8H), 8.38 (s, *para*-phenyl-H, 8H), 7.15 (s, *meta*-phenyl-H, 4H)} spectroscopies. Flash photolysis studies employing **1** were able to resolve the CO rebinding kinetics in both THF and cyclohexane solvents. In CO saturated THF {[CO] $\sim$ 5 mM} and at [**1**] $\cong$ 5 μM, the conversion of [(F_8TPP)Fe^{II}(THF)$_2$] (produced after photolytic displacement of CO) to [(F_8TPP)Fe^{II}(CO)(THF)] was monoexponential, with $k_{obs} = 1.6\ (\pm 0.2) \times 10^4$ s^{-1}. Reduction in [CO] by vigorous Ar purging gave $k_{obs} \cong 10^3$ s^{-1} in cyclohexane. The study presented in this report lays the foundation for applying fast-time scale studies based on CO flash photolysis to the more complicated heterobimetallic heme/Cu systems.

Introduction

In studies of heme proteins including cytochrome *c* oxidase (C*c*O), carbon monoxide has often been exploited to serve as a surrogate for the physiological reactant dioxygen (O_2).[1−12] Such investigations have been extended to CO-adduct formation of model heme systems,[13,14] including the use of carbonmonoxy heme complexes in the study of transient oxygenation after photolytic displacement of the CO ligand.[15] The near ubiquitous use of the carbon monoxide ligand in flash photolysis studies of heme proteins and

---

* To whom correspondence should be addressed. E-mail: karlin@jhu.edu (K.D.K.); meyer@jhu.edu (G.J.M.).

[†] The Johns Hopkins University.

[‡] The University of Delaware.

(1) Varotsis, C.; Zhang, Y.; Appelman, E. H.; Babcock, G. T. *Proc. Natl. Acad. Sci. U.S.A.* **1993**, *90*, 237−241.

(2) Ferguson-Miller, S.; Babcock, G. T. *Chem. Rev.* **1996**, *96*, 2889−2907.

(3) Einarsdottir, O.; Dyer, R. L.; Lemon, D. D.; Killough, P. M.; Hubig, S. M.; Atherton, S. J.; Lopez-Garriga, J. J.; Palmer, G.; Woodruff, W. H. *Biochemistry* **1993**, *32*, 12013−12024.

10.1021/ic026307b CCC: $25.00

model complexes is due to several factors, including its ability to form stable adducts which are resistant to redox changes, its use as a competitive inhibitor of O_2-reduction in both proteins and model complexes, its high quantum yield for photodissociation, and its characteristic intense infrared absorption.

Fast-time scale investigations employing CO flash photolysis have been fruitful for probing the reactivity and dynamics of dioxygen binding and reduction occurring in the heme–copper binuclear active site of C*c*O,[3,16–25] and we wish to extend such studies to our synthetic heme–copper model systems.[26–33] However, in light of the likely difficulty in interpreting data from heterobimetallic heme–copper systems, the elucidation of CO binding and photolysis relating to the individual metal components is essential. While carbon monoxide photodissociation and rebinding in a copper complex used in heme–copper synthetic analogues has been investigated previously,[34] the need for studying the CO chemistry of the tetraarylporphryinate $(F_8TPP)Fe^{II}$ {F_8-TPP = tetrakis(2,6-difluorophenyl)porphyrinate(2−), see diagram, where Ar^F = 2,6-difluorophenyl}[14] is also required.

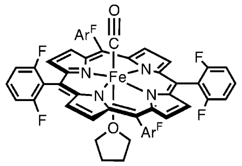

$[(F_8TPP)Fe^{II}(CO)(THF)]$ (**1**)

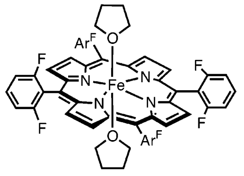

$[(F_8TPP)Fe^{II}(THF)_2]$ (**2**)

Thus, we describe here the synthesis, structural characterization, and laser flash photolysis study of the heme–CO adduct $[(F_8TPP)Fe^{II}(CO)(THF)]$ (**1**) {see diagram}. Furthermore, given the need for understanding ligand binding processes and solvent coordination influences upon reactivity in the ferrous–heme model complex, we have also synthesized the bis-solvento complex, $[(F_8TPP)Fe^{II}(THF)_2]$ (**2**), and its physical and structural characterization is presented here as well.

Experimental Section

Materials and Methods. All reagents and solvents were purchased from commercial sources and were of reagent quality unless otherwise stated. Chromatographic grade alumina (80–200 mesh) was purchased from EM Science. Air-sensitive compounds were handled under argon atmosphere using standard Schlenk techniques, or in an MBraun Labmaster 130 inert atmosphere (<1 ppm O_2, <1 ppm H_2O) glovebox filled with nitrogen. Solvents were distilled over drying agents under argon prior to use: acetonitrile (CH_3CN), propionitrile (CH_3CH_2CN), methylene chloride (CH_2Cl_2), methanol, and heptane from calcium hydride; tetrahydrofuran, diethyl ether, and toluene from sodium/benzophenone; and acetone from Drierite (97% $CaSO_4$, 3% $CoCl_2$). Deoxygenation of these solvents was achieved by bubbling with argon for 30 min, followed by 3 freeze/pump/thaw cycles prior to introduction into the glovebox. NMR solvents were distilled as described and deoxygenated through 5 freeze/pump/thaw cycles. Addition of carbon monoxide (Matheson Gas Products) for UV–vis, infrared (IR), and ^{1}H-, ^{2}H-, and ^{13}C-nuclear magnetic resonance (NMR) spectroscopic studies was effected by direct bubbling through an R & D Separations oxygen/moisture trap model OT3-4 into the sample solution via a syringe needle. ^{13}CO was purchased in 100 mL breakseals from ICON Services, Inc., Marion, NY. Elemental analyses were performed by Desert Analytics, Tucson, AZ.

Synthesis. $(F_8TPP)Fe^{II}$ and its pyrrole-deuterated analogue (F_8-TPP-d_8)Fe^{II} were synthesized according to published procedures.[30,35]

$[(F_8TPP)Fe^{II}(CO)(THF)]\cdot THF$ (1·THF). In the glovebox, to a 100 mL Schlenk flask fitted with a rubber septum was addded a 100 mg sample of $(F_8TPP)Fe^{II}$ dissolved in 10 mL of THF. On the benchtop, the solution was sparged for ~3 min with CO via syringe needle, followed by layering with ~50 mL CO-saturated heptane. After 6 days, lustrous, red crystals suitable for X-ray diffraction

---

(4) Sucheta, A.; Georgiadis, K. E.; Einarsdottir, O. *Biochemistry* **1997**, *36*, 554–565.
(5) Kitagawa, T.; Ogura, T. *Prog. Inorg. Chem.* **1996**, *45*, 431–479.
(6) St. George, R. C. C.; Pauling, L. *Science* **1951**, *114*, 629–634.
(7) Traylor, T. G.; Tsuchiya, S.; Campbell, D. H.; Mitchell, M. J.; Stynes, D. V.; Koga, N. *J. Am. Chem. Soc.* **1985**, *107*, 604–614.
(8) Traylor, T. G.; Magde, D.; Taube, D. J.; Jongeward, K. A. *J. Am. Chem. Soc.* **1987**, *109*, 5864–5865.
(9) Jongeward, K. A.; Magde, D.; Taube, D. J.; Marsters, J. C.; Traylor, T. G.; Sharma, V. S. *J. Am. Chem. Soc.* **1988**, *110*, 380–387.
(10) Hoshino, M.; Nagashima, Y.; Seki, H.; DeLeo, M.; Ford, P. C. *Inorg. Chem.* **1998**, *37*, 2462–2469.
(11) Butler, C. S.; Seward, H. E.; Greenwood, C.; Thomson, A. J. *Biochemistry* **1997**, *36*, 16259–16266.
(12) Miranda, K. M.; Bu, X.; Lorković, I.; Ford, P. C. *Inorg. Chem.* **1997**, *36*, 4838–4848.
(13) Collman, J. P.; Sunderland, C. J.; Boulatov, R. *Inorg. Chem.* **2002**, *41*, 2282–2291.
(14) Kretzer, R. M.; Ghiladi, R. A.; Lebeau, E. L.; Liang, H.-C.; Karlin, K. D. *Inorg. Chem.* **2003**, *42*, 3016–3025.
(15) Momenteau, M.; Reed, C. A. *Chem. Rev.* **1994**, *94*, 659–698.
(16) Babcock, G. T. *Proc. Natl. Acad. Sci., U.S.A.* **1999**, *96*, 12971–12973.
(17) Kitagawa, T.; Ogura, T. *Prog. Inorg. Chem.* **1997**, *45*, 431–479.
(18) Szundi, I.; Liao, G.-L.; Einarsdottir, O. *Biochemistry* **2001**, *40*, 2332–2339.
(19) Han, S.; Takahashi, S.; Rousseau, D. L. *J. Biol. Chem.* **2000**, *275*, 1910–1919.
(20) Giuffre, A.; Forte, E.; Antonini, G.; D'Itri, E.; Brunori, M.; Soulimane, T.; Buse, G. *Biochemistry* **1999**, *38*, 1057–1065.
(21) Woodruff, W. H. *J. Bioenerg. Biomembr.* **1993**, *25*, 177–188.
(22) Koutsoupakis, K.; Stavrakis, S.; Pinakoulaki, E.; Soulimane, T.; Varotsis, C. *J. Biol. Chem.* **2002**, *277*, 32860–32866.
(23) Fiamingo, F. G.; Altschult, R. A.; Moh, P. P.; Alben, J. O. *J. Biol. Chem.* **1982**, *257*, 1639–1650.
(24) Alben, J. O.; Moh, P. P.; Fiamingo, F. G.; Altschult, R. A. *Proc. Natl. Acad. Sci., U.S.A.* **1981**, *78*, 234–237.
(25) Park, S.; Pan, L.-P.; Chan, S. I.; Alben, J. O. *Biophys. J.* **1996**, *71*, 1036–1047.
(26) Ghiladi, R. A.; Ju, T. D.; Lee, D.-H.; Moënne-Loccoz, P.; Kaderli, S.; Neuhold, Y.-M.; Zuberbühler, A. D.; Woods, A. S.; Cotter, R. J.; Karlin, K. D. *J. Am. Chem. Soc.* **1999**, *121*, 9885–9886.
(27) Ghiladi, R. A.; Hatwell, K. R.; Karlin, K. D.; Huang, H.-w.; Moënne-Loccoz, P.; Krebs, C.; Huynh, B. J.; Marzilli, L. A.; Cotter, R. J.; Kaderli, S.; Zuberbühler, A. D. *J. Am. Chem. Soc.* **2001**, *123*, 6183–6184.
(28) Ghiladi, R. A.; Karlin, K. D. *Inorg. Chem.* **2002**, *41*, 2400–2407.
(29) Ju, T. D.; Ghiladi, R. A.; Lee, D.-H.; van Strijdonck, G. P. F.; Woods, A. S.; Cotter, R. J.; Young, J. V. G.; Karlin, K. D. *Inorg. Chem.* **1999**, *38*, 2244–2245.
(30) Kopf, M.-A.; Neuhold, Y.-M.; Zuberbühler, A. D.; Karlin, K. D. *Inorg. Chem.* **1999**, *38*, 3093–3102.
(31) Kopf, M.-A.; Karlin, K. D. *Inorg. Chem.* **1999**, *38*, 4922–4923.
(32) Kopf, M.-A.; Karlin, K. D. In *Biomimetic Oxidations*; Meunier, B., Ed.; Imperial College Press: London, 2000; Chapter 7, pp 309–362.
(33) Kim, E.; Helton, M. E.; Wasser, I. M.; Karlin, K. D.; Lu, S.; Huang, H.-w.; Moënne-Loccoz, P.; Incarvito, C. D.; Rheingold, A. L.; Honecker, M.; Kaderli, S.; Zuberbühler, A. D. *Proc. Natl. Acad. Sci. U.S.A.* **2003**, *100* (7), 3623–3628.
(34) Scaltrito, D. V.; Fry, H. C.; Showalter, B. M.; Thompson, D. W.; Liang, H.-C.; Zhang, C. X.; Kretzer, R. M.; Kim, E.-i.; Toscano, J. P.; Karlin, K. D.; Meyer, G. J. *Inorg. Chem.* **2001**, *40*, 4514–4515.
(35) Ghiladi, R. A.; Kretzer, R. M.; Guzei, I.; Rheingold, A. L.; Neuhold, Y.-M.; Hatwell, K. R.; Zuberbühler, A. D.; Karlin, K. D. *Inorg. Chem.* **2001**, *40*, 5754–5767.

were obtained; crystallographic analysis later revealed a formulation of [$(F_8TPP)Fe^{II}(CO)(THF)$]·3THF (**1·3THF**) for these crystals. A purple powder, **1·THF**, was obtained by rapid addition of an excess of heptane to the THF solution (5:1; v/v, both CO saturated) containing $(F_8TPP)Fe^{II}$ followed by gravity filtration under an inert atmosphere. The isolated solid was kept under a CO atmosphere to prevent loss of the carbonyl ligand. Analysis of the noncrystalline material follows. UV−vis (THF; λ_{max}, nm): 411 nm, 525 nm. ^1H NMR (CD_3CN): δ 8.82 (s, pyrrole-H, 8H), 7.89 (s, *para*-phenyl-H, 8H), 7.46 (s, *meta*-phenyl-H, 4H), 3.58 (s, THF, 8H), 1.73 (s, THF, 8H). Anal. Calcd for [$(F_8TPP)Fe^{II}(CO)(THF)$]·1THF, $C_{53}H_{36}F_8FeN_4O_3$: C, 63.41; H, 3.66; N, 5.69. Found: C, 63.91; H, 3.38; N, 6.03.

[$(F_8TPP)Fe^{II}(THF)_2$]·THF (2·THF). The bis-tetrahydrofuran analogue of $(F_8TPP)Fe^{II}$ was prepared by dissolution of 54 mg of $(F_8TPP)Fe^{II}$ in 10 mL deoxygenated THF in a glovebox. The THF/porphyrin solution was layered with an equal volume of heptane. After 3 days, dark purple/blue crystals suitable for X-ray diffraction were obtained; crystallographic analysis later revealed a formulation of [$(F_8TPP)Fe^{II}(THF)_2$]·2THF (**2·2THF**) for this crystalline material. A noncrystalline purple solid of **2·THF** was obtained by rapid addition of an excess (5:1, v/v) of heptane to the THF solution containing $(F_8TPP)Fe^{II}$, followed by gravity filtration under an inert atmosphere. Analysis of the powder material follows. UV−vis (THF; λ_{max}, nm): 421 nm, 542 nm. ^1H NMR (THF-d_8): δ 56.7 (s, pyrrole-H, 8H), 8.38 (s, *para*-phenyl-H, 8H), 7.15 (s, *meta*-phenyl-H, 4H). Anal. Calcd for [$(F_8TPP)Fe^{II}(THF)_2$]·THF, $C_{56}H_{44}F_8FeN_4O_3$: C, 65.37; H, 4.28; N, 5.45. Found: C, 64.72; H, 4.10; N, 5.35.

Infrared Spectroscopy. IR spectra were obtained at room temperature using a Mattson Galaxy 4030 series FT-IR spectrophotometer. IR samples were prepared in a drybox by dissolving 5−10 mg of $(F_8TPP)Fe^{II}$ in ~1 mL of solvent in a glass vial, which was subsequently sealed with a rubber septum prior to removal to the benchtop. After an IR spectrum was taken using a SPECAC solution cell of the $(F_8TPP)Fe^{II}$ as a control, the stock solution in the vial was bubbled with CO for 5−10 s. An IR spectrum was then taken of the carbonylated species in order to observe the specific $\nu(CO)_{Fe}$.

Laser Flash Photolysis Studies. Transient absorbance measurements were performed on a previously described apparatus.[36] Excitation was carried out using the 532 or 417 nm laser pulses, ca. 8 nm and 1−30 mJ cm^{-2}, from a Nd:YAG (Continuum Surelite II or III) laser (with a H_2-filled Raman shifter for 417 nm excitation). The sample was protected from the probe light using a fast shutter and appropriate UV and heat absorbing glass and solution filter combinations. In general, kinetic traces represent the average of 10−160 laser shots, typically 40. Samples were prepared in the inert atmosphere of a glovebox, and cuvettes were stoppered with a rubber septum, which was pierced with a noncoring needle for CO bubbling.

Crystallographic Studies. Crystal, data collection, and refinement parameters are given in Table 1. The systematic absences in the diffraction data for **1** were uniquely consistent for the orthorhombic space group $P2_12_12_1$, and the data for **2** were consistent with the space groups $C2/c$ and Cc. E-statistics, as well as the presence of an inversion center of **2**, suggested the centrosymmetric option, which yielded chemically reasonable and computationally stable results of refinement. The structures were solved using direct methods, completed by subsequent difference Fourier syntheses and refined by full-matrix least-squares procedures. The asymmetric unit of **1** contains two independent, but chemically equivalent, iron complexes. Platon/Squeeze[37] was applied to **1** to resolve three THF molecules (120 electrons) per complex. Within the 2018.9 Å^3 void space occupied by solvent molecules per unit cell, a total of 985 electrons were found. In this treatment of solvent, the contribution of the solvent molecule is treated collectively and is not refined as individual atoms. The R factor for **1** was significantly reduced when refined as 87/13 racemic mixture. All phenyl rings of **1** were fixed as rigid planar groups. The asymmetric unit of **2** contains half of an Fe complex which lies on an inversion center and two halves of THF molecules, one of which is equally distorted over two positions. All non-hydrogen atoms in both structures were refined with anisotropic displacement coefficients. All hydrogen atoms, except those bonded with the distorted THF molecule for **2**, were treated as idealized contributions.

Table 1. Crystal Data and Structure Refinement for [$(F_8TPP)Fe^{II}(CO)(THF)$]·3THF (**1·3THF**) and [$(F_8TPP)Fe^{II}(THF)_2$]·2THF (**2·2THF**)

	[$(F_8TPP)Fe^{II}$ (CO)-(THF)]·3THF (**1·3THF**)	[$(F_8TPP)Fe^{II}$ $(THF)_2$]·2THF (**2·2THF**)
formula	$C_{61}H_{52}F_8FeN_4O_5$	$C_{60}H_{52}FeN_4O_4$
fw	1128.92	1100.91
space group	$P2_12_12_1$	$C2/c$
a, Å	11.7908(2)	21.3216(3)
b, Å	20.4453(2)	12.1191(2)
c, Å	39.9423(3)	21.0125(2)
β, deg		105.3658(5)
V, Å^3	9628.7(2)	5235.51(9)
Z	8	4
cryst color, habit	deep red plate	dark blue plate
D(calcd), g cm^3	1.558	1.397
μ(Mo Kα), cm^{-1}	4.05	3.69
temp, K	203(2)	173(2)
diffractometer	Siemens P4/CCD	Siemens P4/CCD
radiation	Mo Kα ($\lambda = 0.71073$ Å)	Mo Kα ($\lambda = 0.71073$ Å)
$R(F)$, %	8.98	6.66
$R(wF^2)$,[a] %	23.56	19.38

[a] Quantity minimized = $R(wF^2) = \sum[w(F_o^2 - F_c^2)^2]/\sum[(wF_o^2)_2]^{1/2}$; $R = \sum\Delta/\sum(F_o)$, $\Delta = |(F_o - F_c)|$.

All software and sources of the scattering factors are contained in the SHELXTL (version 5.10) program library (G. Sheldrick, Siemens XRD, Madison, WI).

Results and Discussion

Synthesis. The carbonmonoxy−THF complex [$(F_8TPP)Fe^{II}(CO)(THF)$]·3THF (**1·3THF**) was prepared by dissolving a pure sample of $(F_8TPP)Fe^{II}$ in deaerated THF, followed by carbonylation via direct bubbling of CO for several minutes. Crystalline material suitable for X-ray diffraction study with the structurally deduced formula **1·3THF** was obtained by slow precipitation from a CO-saturated THF/heptane cosolvent system. This six-coordinate, low-spin (vide infra) Fe^{II} complex has been characterized: X-ray crystallography and IR spectroscopy are presented here, while UV−vis and $^{1,2}H$/^{13}C NMR discussions (including Experimental Methods) are given in the Supporting Information. Elemental analysis on the noncrystalline material obtained from rapid precipitation of the heme−CO adduct confirms the loss of two molecules of THF (solvent) when compared to the

---

(36) Kelly, C. A.; Thompson, D. W.; Farzad, F.; Meyer, G. J. *Langmuir* **1999**, *15*, 731.

(37) Spek, A. L. *Acta Crystallogr., Sect. A* **1990**, *46*, C34.

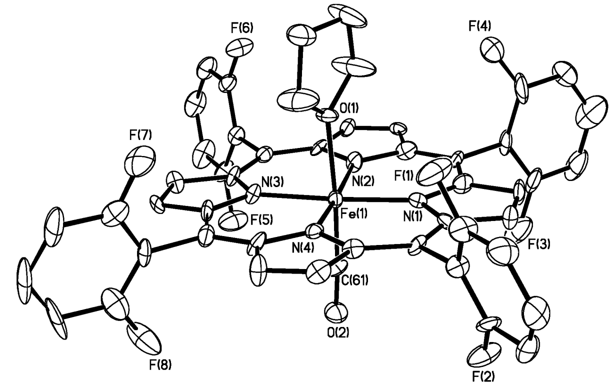

Figure 1. ORTEP (30% ellipsoids) diagram of [(F_8TPP)Fe^{II}(CO)(THF)]·3THF (**1·3THF**). Hydrogen atoms and two molecules of THF (solvent, nonbinding) are omitted for clarity.

crystalline product, for a formulation of [(F_8TPP)Fe^{II}(CO)(THF)]·1THF (**1·THF**); this result is supported by the ^{1}H NMR solution study in CD_3CN which shows only 2 THF molecules present in the noncrystalline material. Complex **1** dissolves in CH_2Cl_2 and THF and is sparingly soluble in toluene and benzene. In CH_3CN and CH_3CH_2CN, the THF axial base is likely replaced by the nitrile solvent, but the CO ligand remains bound to the iron site for extended periods as evidenced by solution infrared studies (see following paragraphs).

Since we were investigating ligand and solvent coordination influences upon the properties of (F_8TPP)Fe^{II}, we also synthesized the bis-tetrahydrofuran analogue [(F_8TPP)Fe^{II}(THF)$_2$] (**2**) to compare iron−ligand (axial) and iron−porphyrin structural parameters. The axial THF ligand was chosen because it is a weak-field, weakly coordinating ligand. Dissolution of (F_8TPP)Fe^{II} in deoxygenated THF under an inert atmosphere gave a deep purple-red solution, which yielded dark purple crystals upon layering with deaerated heptane; X-ray diffraction study of the crystalline material yielded the structurally deduced formulation of [(F_8TPP)Fe^{II}(THF)$_2$]·2THF (**2·2 THF**). A noncrystalline purple solid was obtained by rapid addition of an excess (5:1, v/v) of heptane to the THF solution; elemental analysis revealed a formulation of [(F_8TPP)Fe^{II}(THF)$_2$]·1THF (**2·1 THF**), a loss of one THF solvent molecule compared to the crystalline material. As with complex **1**, the bis-THF adduct **2** dissolves in CH_2Cl_2 and THF and is sparingly soluble in toluene and benzene. However, in CH_3CN and CH_3CH_2CN, both axial THF ligands are lost, and a five-coordinate, high-spin species with a nitrile axial ligand is generated.

X-ray Crystal Structure Determination of [(F_8TPP)Fe^{II}(CO)(THF)]·3THF (1·3THF) and [(F_8TPP)Fe^{II}(THF)$_2$]·2THF (2·2THF). Details of the data collection and refinement parameters for **1·3THF** and **2·2THF** are provided in Table 1 and the Supporting Information. Figures 1 and 2 show the ORTEP diagrams (30% ellipsoids) of **1·3 THF** and **2·2 THF**, respectively, and a summary of selected bond distances and angles is provided in Tables 2 and 3. The crystal structures of **1** and **2** both indicate six-coordinate Fe^{II} centers with ligation to the four-coordinate porphyrin and two axial ligands in each case. In **1**, CO and a solvent THF molecule provide axial ligation, while two THF molecules serve as ligands for the axial sites in **2**. In **1**, the Fe atom is pulled out of the porphyrin plane slightly toward the tightly bound CO ligand. In **2**, the two axial THF ligands are related by a center of inversion with a linear angle between axial ligands (180.0°) and a near centering of the Fe atom in the porphyrin plane. Neither complex **1** or **2** shows any significant ruffling of the porphyrin from planarity.

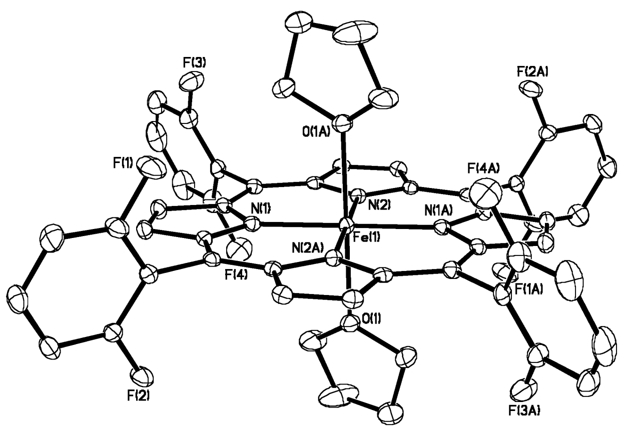

Figure 2. ORTEP (30% ellipsoids) diagram of [(F_8TPP)Fe^{II}(THF)$_2$]·2THF (**2·2THF**). Hydrogen atoms and two molecules of THF (solvent, nonbinding) are omitted for clarity.

Table 2. Selected Distances (Å) and Angles (deg) for [(F_8TPP)Fe^{II}(CO)(THF)]·3THF (**1·3THF**)

	Intramolecular Distances (Å)		
O(2)−C(61)	1.141(7)	Fe(1)−C(61)	1.755(6)
Fe(1)−O(1)	2.121(4)	Fe(1)−N(1)	1.978(5)
Fe(1)−N(2)	2.022(5)	Fe(1)−N(3)	2.021(4)
Fe(1)−N(4)	1.979(5)		
	Intramolecular Angles (deg)		
O(2)−C(61)−Fe(1)	176.1(5)	C(61)−Fe(1)−O(1)	175.0(2)
C(61)−Fe(1)−N(1)	93.0(2)	C(61)−Fe(1)−N(2)	95.8(2)
C(61)−Fe(1)−N(3)	89.9(2)	C(61)−Fe(1)−N(4)	89.7(2)
N(1)−Fe(1)−O(1)	89.57(19)	N(2)−Fe(1)−O(1)	88.48(19)
N(3)−Fe(1)−O(1)	87.58(19)	N(4)−Fe(1)−O(1)	86.03(18)
N(1)−Fe(1)−N(2)	90.23(19)	N(1)−Fe(1)−N(3)	177.1(2)
N(1)−Fe(1)−N(4)	89.8(2)	N(3)−Fe(1)−N(2)	89.4(2)
N(4)−Fe(1)−N(2)	174.5(2)	N(4)−Fe(1)−N(3)	90.31(18)

Table 3. Selected Distances (Å) and Angles (deg) for [(F_8TPP)Fe^{II}(THF)$_2$]·2THF (**2·2THF**)

	Intramolecular Distances (Å)		
Fe(1)−O(1)	2.314(3)	Fe(1)−N(1)	2.061(3)
Fe(1)−N(2)	2.074(3)		
	Intramolecular Angles (deg)		
O(1A)−Fe(1)−O(1)	180.0	N(1)−Fe(1)−O(1)	90.43(10)
N(1A)−Fe(1)−O(1)	89.57(10)	N(2)−Fe(1)−O(1)	88.79(10)
N(2A)−Fe(1)−O(1)	91.20(10)	N(1)−Fe(1)−N(1A)	179.997(1)
N(1)−Fe(1)−N(2)	89.87(11)	N(1)−Fe(1)−N(2A)	90.13(11)

The average Fe−$N_{porphyrin}$ distances are 2.00 Å in **1** and 2.07 Å in **2**. These values are consistent with other Fe−$N_{porphyrin}$ bond lengths for low- and high-spin (respectively) ferrous species (Table 4).[38,39] Comparable core expansion of the hexacoordinate, high-spin [(TPP)Fe^{II}(THF)$_2$] species is observed with an average Fe−$N_{porphyrin}$ distance of 2.06 Å. All of the diamagnetic, low-spin complexes have an

---

(38) Reed, C. A.; Mashiko, T.; Scheidt, W. R.; Spartalian, K.; Lang, G. *J. Am. Chem. Soc.* **1980**, *102*, 2302−2306.

(39) Scheidt, W. R.; Reed, C. A. *Chem. Rev.* **1981**, *81*, 543−555.

Table 4. Comparative Data for Fe^{II} Heme Model Compounds

compd	$Fe-C_{CO}$, Å	C−O, Å	$O_{CO}-C_{CO}-Fe$, deg	$C_{CO}-Fe-O_{ax}$ or $C_{CO}-Fe-N_{ax}$, deg	av. $Fe-N_{porph}$, Å	$Fe-O_{ax}$ or $Fe-N_{ax}$, Å	ν_{CO} (solvent), cm^{-1}
$[(F_8TPP)Fe^{II}(THF)_2]$[a]					2.07	2.314(3)	
$[(TPP)Fe^{II}(THF)_2]$[38]					2.06	2.351(3)	
$[(TPP)Fe^{II}(Pip)_2]$[54]					2.004(4)	2.127(3)	
$[(TPP)Fe^{II}(1\text{-}MeIm)_2]$[55]					1.997(4)	2.014(5)	
$[(THFPP)Fe^{II}(py)_2]$[56]					1.958(6)	2.001(6)	
$[(F_8TPP)Fe^{II}(THF)(CO)]$[a]	1.755(6)	1.141(7)	176.1(5)	175.0(2)	2.00	2.121(4)	1979 (THF)
$[(TPP)Fe^{II}(CO)(py)]$[57]	1.77(2)	1.12(2)	179(2)	177.5(8)	2.02(3)	2.10	1980
$[(deut)Fe^{II}(THF)(CO)]$[42]	1.706(5)	1.144(5)	178.3(14)	177.4(9)	1.98	2.127(4)	1955 (KBr)
$[(C_2\text{-}Cap)Fe^{II}(CO)(1\text{-}MeIm)]$[58]	1.742(7)	1.161(8)	172.9(6)	174.7(3)	1.990(7)	2.043(6)	2002 (Nujol)
$[(C_2\text{-}Cap)Fe^{II}(CO)(1\text{-}MeIm)]$[58]	1.748(7)	1.158(8)	175.9(6)	177.8(3)	1.988(13)	2.041(5)	2002 (Nujol)

[a] This work. Abbreviations used: TPP = *meso*-tetraphenylporphyrin; Pip = piperidine; 1-MeIm = *N*-methylimidazole; THFPP = 5,10,15,20-tetrakis(heptafluoropropyl)porphyrin; py = pyridine; deut = deuteroporphyrin; C_2-Cap = 5,10,15,20-[pyromellitoyl(tetrakis(*o*-oxyethoxyphenyl))]porphyrin.

average $Fe-N_{porphyrin}$ distance between 1.96 and 2.02 Å. The increase in average bond length for a high-spin ferrous species is consistent with the population of the $3d_{x^2-y^2}$ orbital in both complex **1** and $[(TPP)Fe^{II}(THF)_2]$.[40]

The $Fe-O_{THF}$ distance in the heme−CO adduct **1** is 2.121(4) Å but is elongated by ∼0.19 Å in **2**. The shorter bond in **1** and in $[(deut)Fe^{II}(CO)(THF)]$ compared to other low-spin six-coordinate hemes (without a CO ligand) (Tables 3 and 4) is expected because of the *trans* effect of CO. The especially long 2.314(3) Å $Fe-O_{THF}$ distance in **2** is consistent with the population of the $3d_{z^2}$ orbital as required by the high-spin ground state of this complex. The relatively long $Fe-O_{THF}$ bond distance in all of these examples is consistent with the assignment of THF as a weak-field, weakly binding ligand. By contrast, the bond length between Fe^{II} and strongly coordinating axial ligands is shorter by ∼0.2−0.3 Å, as in the bis-piperdine, 1-methylimidazole, and pyridine complexes (Table 4), when compared to the bis-THF systems. The carbonyl CO bond distance of 1.141(7) Å in **1** is consistent with that of other $Fe^{II}-CO$ porphyrin complexes (Table 4). The tight binding of the carbonyl is indicated by the short $Fe-C_{(CO)}$ bond distance of 1.755(6) Å, which is also in the expected range for low-spin carbonyl heme complexes.

The Fe−CO unit prefers a linear geometry in order to maximixe the Fe $d\pi \rightarrow$ CO π^* back-bonding.[41] Two angles which are significant with respect to defining linearity of the CO are given as θ, the deviation of the Fe−C bond from perpendicularity relative to the porphrin plane, and ϕ, the angle of the CO bond relative to the Fe−C bond (see diagram). In **1**, θ is 5°, and ϕ is 3.9°. The combination of these two angles leads to a 0.33 Å deviation from perpendicularity of the O atom. For comparison, θ is 2.6° and ϕ is 1.7° in $[(deut)Fe^{II}(CO)(THF)]$, leading to only a 0.16 Å displacement of the O atom from the perpendicular position. Although **1** is more densely packed than $[(deut)Fe^{II}(CO)(THF)]$, crystallographic packing forces are not completely responsible for the differences in geometry as evidenced by the large differences in the CO stretching frequency in solution (see IR discussion). The bending and tilting of **1** is more consistent with the angles observed for sterically blocked, capped porphyrins (Table 4). The geometry of **1** represents one of the largest tilt and bend combinations observed for an unblocked heme model complex.

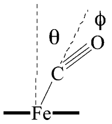

IR Spectroscopy. Solution cell IR spectra of **1** reveal a single CO stretch in the typical region for six-coordinate, low-spin Fe(II)−porphyrin complexes (Table 4), with ν_{CO} = 1979 cm^{-1} in THF, 1976 cm^{-1} in acetone, and 1982 cm^{-1} in acetonitrile. Although the vibrational frequencies of the Fe−CO unit are generally thought of as useful indicators of the *trans* ligand interactions with the iron heme, the CO stretch does not correlate well with the base strength of the solvent in this case. Other complexes believed to have strong axial ligation also fall in the region between 1980 and 2000 cm^{-1}.

For comparison, the complex $[(deut)Fe^{II}(CO)(THF)]$ produced a particularly low energy CO stretch at 1955 cm^{-1} in KBr and 1962 cm^{-1} in THF.[42] The difference in the CO stretching frequency between **1** and $[(deut)Fe^{II}(CO)(THF)]$ is significant. The most likely explanation is the nature of the difference in the porphyrins, leading to variations in Fe−C bond lengths; $[(deut)Fe^{II}(CO)(THF)]$ has a stronger Fe−C bond (Table 4), leading to a weaker C−O bond (and lower ν(CO)).[43] Another influence may be the larger deviation from linearity of the Fe−CO group with **1**, giving rise to poorer overlap between the Fe $d\pi$ and CO π^* orbitals. Electron-withdrawing fluorines in F_8-TPP in **1** also lead to less CO back-bonding.

Axial Ligand Substitution Kinetics. Rapid visible spectral changes are observed when $[(F_8TPP)Fe^{II}(THF)_2]$ in THF is anaerobically treated with CO, Figure 3. The spectral changes are assigned to the reaction given in eq 1.

The kinetics for the reaction of $[(F_8TPP)Fe^{II}(THF)_2]$ (**2**) with CO were on a time scale amenable for study by nanosecond time-resolved absorption "flash and trap" tech-

---

(40) Scheidt, W. R. *Acc. Chem. Res.* **1977**, *10*, 339−345.

(41) Cotton, F. A.; Wilkinson, G. *Advanced Inorganic Chemistry*, 5th ed.; John Wiley: New York, 1988.

(42) Scheidt, W. R.; Haller, K. J.; Fons, M.; Mashiko, T.; Reed, C. A. *Biochemistry* **1981**, *20*, 3653−3657.

(43) We thank a reviewer for pointing out this explanation.

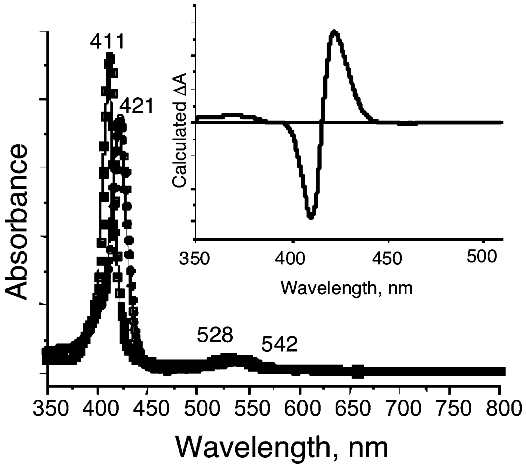

Figure 3. Ground state absorption spectra of [(F_8TPP)Fe^{II}(CO)(THF)] (**1**) (■) and [(F_8TPP)Fe^{II}(THF)$_2$] (**2**) (●) in neat THF. The inset represents the calculated absorption difference spectra as found by Abs[(F_8TPP)Fe^{II}(THF)$_2$] − Abs[(F_8TPP)Fe^{II}(CO)(THF)].

$$[(F_8TPP)Fe^{II}(THF)_2] + CO \leftrightarrow [(F_8TPP)Fe^{II}(CO)(THF)] + THF \quad (1)$$

niques similar to those used in previous reports.[15,44−46] Described in the following paragraphs are the results of kinetic studies on the reaction given in eq 1, in both THF and cyclohexane media followed by a proposed mechanistic model.

Absorption difference spectra measured after pulsed laser excitation of [(F_8TPP)Fe^{II}(CO)(THF)] (**1**) (∼10^{-5} M) in CO-saturated THF ([CO] ∼ 5 mM) are shown in Figure 4. We note that either 417 or 532 nm laser excitation yielded identical absorption difference spectra. The spectrum shows a sharp bleach, i.e., negative absorption change, at 415 nm and a positive absorption band at 430 nm. The spectral features are consistent with CO loss and the immediate appearance of [(F_8TPP)Fe^{II}(THF)$_2$] (**2**). In support of this assignment, the calculated absorption difference spectrum, determined by subtracting the ground state spectrum of [(F_8TPP)Fe^{II}(THF)$_2$] (**2**) from that of [(F_8TPP)Fe^{II}(CO)(THF)] (**1**) (inset Figure 3) shows a similar profile to that of transiently observed absorption difference spectrum.

The CO photodissociation and the trapping by THF are rapid and occur within the instrument response function, <10 ns. The absorption spectral changes observed for the conversion of [(F_8TPP)Fe^{II}(THF)$_2$] (**2**) to [(F_8TPP)Fe^{II}(CO)(THF)] (**1**) in neat THF under 1 atm of CO were monoexponential and returned cleanly to ground state products with a rate constant, $k_{obs} = 1.6\ (\pm\ 0.2) \times 10^4\ s^{-1}$. Ground state absorbance measurements taken before and after pulsed laser experiments gave no evidence of sample decomposition. Reduction of the CO concentration by vigorous Ar purging reduced k_{obs} to ∼10^3 s^{-1}.

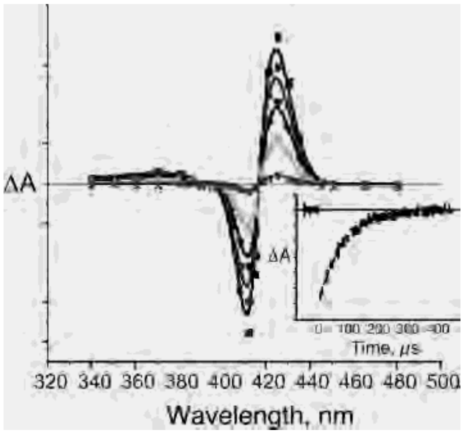

Figure 4. Absorption difference spectra obtained after pulsed 532 nm light excitation of in carbon monoxide saturated THF. The spectra were recorded at the following delay times: 0 μs (■), 20 μs (●), 50 μs (▼), 100 μs (◆), and 240 μs (×). The inset shows an absorption transient acquired at 415 nm with a superimposed fit to a first-order kinetic model.

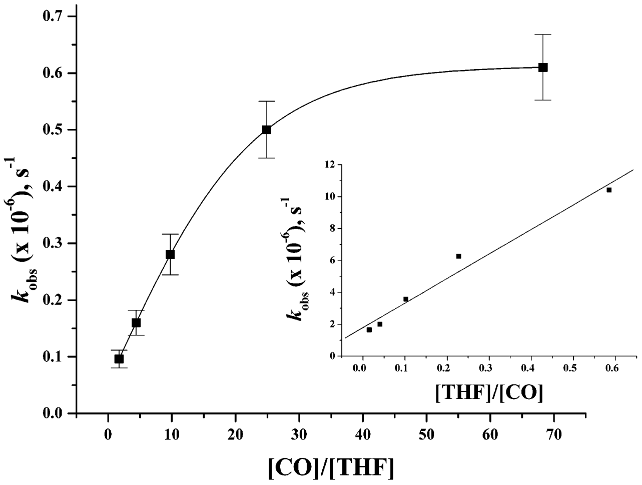

Figure 5. The observed rate constant for eq 1 as a function of [CO]/[THF] in cyclohexane. The inset shows a double reciprocal plot of the same data.

To gain additional insight into the kinetic processes that occur after laser excitation, CO recombination kinetics were studied in cyclohexane as a function of THF concentration. Cyclohexane was chosen because it is noncoordinating, does not π-stack with porphyrins, and should not significantly alter the kinetic rate constant for THF binding. Transient signals were monitored at 427 and 410 nm in cyclohexane over a THF concentration range 1 mM to 1 M. The observed rate constants determined by analysis of the time dependent absorption changes at 410 and 427 nm were found to decrease with increasing [THF] ([CO] ∼ 5 mM) and finally became independent of [THF] when [THF] > 0.30 M, Figure 5.

Mechanistic Model for Ligand Substitution Reactions. Scheme 1 summarizes the proposed mechanism for CO photodissociation and rebinding. Note that we have adopted the notation of Stynes, where the *trans* ligand is indicated as a superscript and the leaving (−) or entering (+) groups as a subscript.[45,46]

Pulsed laser excitation into either the Soret or α band of [(F_8TPP)Fe^{II}(CO)(THF)] (**1**) produces a photodissociative excited state, [(F_8TPP)Fe^{II}(CO)(THF)]*. Previous studies of [(heme)Fe^{II}(His)(CO)], where His is histidine, have estab-

---

(44) Traylor, T. G. *Acc. Chem. Res.* **1981**, *14*, 102−113.
(45) Thompson, D. W.; Stynes, D. V. *Inorg. Chem.* **1991**, *30*, 636−640.
(46) Thompson, D. W.; Stynes, D. V. *Inorg. Chem.* **1990**, *29*, 3815−3822.

Scheme 1

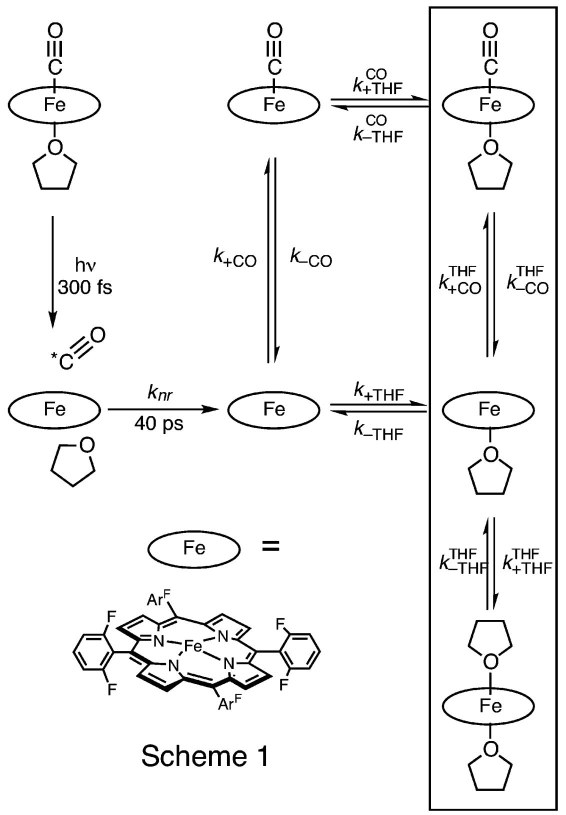

lished that both the His and CO ligands are photodissociated in the excited state on a 300 fs time scale to yield a four-coordinate "bare" heme.[47] Similar dynamics are assumed to occur in this work since THF is a weaker ligand for Fe(II) when compared to histidine. We note that stronger-field ligands, such as isocyanides, are apparently retained after photolysis.[48,49] Upon ligand dissociation, the excited heme relaxes nonradiatively in ∼40 ps to yield the four-coordinate heme.[47]

Mechanistically, the bare four-coordinate heme present after photolysis and excited state relaxation can react with either CO or THF. Geminate recombination of hemes and the photodissociated ligands occurs on a time scale too fast to be measured by our apparatus.[50] If geminate CO rebinding occurs, no spectral changes would be observed. Ford and Traylor have shown that most ligands react with unsaturated hemes with diffusion controlled rates while CO differs significantly with activation control in low viscosity solvents.[51] The data reported here in neat THF are consistent with rapid trapping to form $[(F_8TPP)Fe^{II}(THF)_2]$ within 10 ns. At low THF concentrations in cyclohexane, a rapid equilibrium appears to exists between the mono- and bis-THF compounds.[52] Therefore, the species present on nanosecond and longer time scales are the mono- and bis-THF adducts and the carbonyl compound shown in the box on the right-hand side of Scheme 1. The equilibrium constants for CO and THF binding in a related heme (deuteroheme) have been determined to be 5×10^4 M^{-1} and 5.2 M^{-1}, respectively.[53]

There is an overwhelming body of evidence in support of a dissociative (D) mechanism for CO coordination to a six-coordinate heme.[15,44−46] For a reaction proceeding through a D mechanism, k_{obs} is not an elementary rate constant and is given by eq 2.

$$k_{obs} = \frac{k_{-THF}^{THF}\, k_{+CO}^{THF}[CO] + k_{-CO}^{THF}\, k_{+THF}^{THF}[THF]}{k_{+CO}^{THF}[CO] + k_{+THF}^{THF}[THF]} \qquad (2)$$

The kinetic terms in eq 2 are defined in Scheme 1.[15,44−46] In THF solution, where [THF] ≫ [CO] and k_{-CO} is small, the reaction proceeds to completion, and eq 2 simplifies to

$$k_{obs} = k_f[CO] \qquad (3)$$

where

$$k_f = \frac{k_{-THF}^{THF}\, k_{+CO}^{THF}}{k_{+THF}^{THF}[THF]} \qquad (4)$$

With $k_{obs} = 1.6\ (\pm 0.2) \times 10^4\ s^{-1}$ and [CO] $\sim 5 \times 10^{-3}$ M, k_f is calculated to be $3.2 \times 10^6\ M^{-1}\ s^{-1}$. The forward rate constants for eq 1 depend on the lability of THF and the relative rate parameters $k_{+CO}^{THF}/k_{+THF}^{THF}$. The $[(F_8TPP)Fe^{II}(THF)_2]$ complex is high spin, and the rate constants for axial ligand substitution are expected to be large. This point will be elaborated upon in the following paragraphs.

Reaction 1 was also studied in cyclohexane with added THF to fully establish the dissociative mechanism and to provide a kinetic rate constant for THF dissociation. The observed rate constant displays a linear dependence on [CO]/[THF] under conditions where the [CO]/[THF] ratio approaches zero. Equations 3 and 4 can be rearranged to give eq 5.

$$k_{obs}^{\ -1} = \left(\frac{1}{k_{-THF}^{THF}}\right)\left(\frac{k_{+THF}^{THF}}{k_{+CO}^{THF}}\right)\left(\frac{[THF]}{[CO]}\right) + \left(\frac{1}{k_{-THF}^{THF}}\right) \qquad (5)$$

Plots of the kinetic data to eq 5 (inset in Figure 5) were found to be linear with a slope 1.5×10^{-5} s and an intercept

---

(47) Huang, Y.; Marden, M. C.; Lambry, J.-C.; Fontaine-Aupart, M.-P.; Pansu, R.; Martin, J.-L.; Poyart, C. *J. Am. Chem. Soc.* **1991**, *113*, 9141−9144.

(48) Dixon, D. W.; Kirmaier, C.; Holten, D. *J. Am. Chem. Soc.* **1985**, *107*, 808−813.

(49) Taube, D.; Traylor, T. G.; Magde, D.; Walda, K.; Luo, J. *J. Am. Chem. Soc.* **1992**, *114*, 9182−9188.

(50) Traylor, T. G.; Magde, D.; Luo, J.; Walda, K. N.; Bandyopadhyay, D.; Wu, G. Z.; Sharma, V. S. *J. Am. Chem. Soc.* **1992**, *114*, 9011−9017.

(51) Traylor, T. G.; Luo, J.; Simon, J. A.; Ford, P. C. *J. Am. Chem. Soc.* **1992**, *114*, 4340−4345.

(52) We note that Reed et al. (ref 38) suggest that the structurally characterized complex $[(TPP)Fe^{II}(THF)_2]$ is most likely five-coordinate in THF solution.

(53) Rougee, M.; Brault, D. *Biochemistry* **1975**, *14*, 4100−4106.

(54) Radonovich, L. J.; Bloom, A.; Hoard, J. L. *J. Am. Chem. Soc.* **1972**, *94*, 2073−2078.

(55) Jameson, G. B.; Molinaro, F. S.; Ibers, J. A.; Collman, J. P.; Brauman, J. I.; Rose, E. J.; Suslick, K. S. *J. Am. Chem. Soc.* **1980**, *102*, 3224−3237.

(56) Moore, K. T.; Fletcher, J. T.; Therien, M. J. *J. Am. Chem. Soc.* **1999**, *121*, 5196−5209.

(57) Peng, S.-M.; Ibers, J. A. *J. Am. Chem. Soc.* **1976**, *98*, 8032−8036.

(58) Kim, K.; Ibers, J. A. *J. Am. Chem. Soc.* **1991**, *113*, 6077−6081.

1.8×10^{-6} s. From these data, the limiting off rate of THF was determined to be $k_{-THF}^{THF} = 5.6 \times 10^{5}$ s^{-1} and $k_{+CO}^{THF}/k_{+THF}^{THF} = 0.12$. The saturation kinetics observed at higher THF concentrations are fully consistent with a D mechanism whereby THF dissociation from [(F$_8$TPP)Fe^{II}(THF)$_2$] to generate the five-coordinate transient intermediate, [(F$_8$TPP)-Fe^{II}(THF)], is the rate determining step for CO rebinding. The saturation kinetics also provide compelling evidence that a six-coordinate THF complex is obtainable in solution. A comparison with the literature data reveals that [(F$_8$TPP)-Fe^{II}(THF)$_2$] has some of most labile axial ligands known for heme porphryins.[15,44−46]

Conclusions

We have synthesized and structurally characterized both the heme−CO adduct [(F$_8$TPP)Fe^{II}(THF)(CO)] (**1**) and the bis-THF adduct [(F$_8$TPP)Fe^{II}(THF)$_2$] (**2**). Both complexes were shown to be six-coordinate in the solid state. We also present evidence that **2** is a six-coordinate high-spin ferrous heme in solution. Complex **1** proved amenable to study by fast-time scale UV−vis spectroscopy as initiated by flash photolysis, and we have provided a reasonable mechanism which describes the kinetics of CO-dissociation (photolytic) and rebinding in the weakly coordinating THF solvent. The use of weak-field ligands in nominally noncoordinating solvents (cyclohexane) allows for the study of four-coordinate hemes (upon photolysis) and may be potentially useful as probes to mimic active sites in a number of iron-containing enzymes. Furthermore, the results presented here lay the foundation for similar studies involving the more complicated carbonyl adducts of heterobimetallic complexes as models for the active site of cytochrome *c* oxidase, and such studies are now in progress.

Acknowledgment. This research was supported by the National Institutes of Health (Grants GM28962 and GM60353 to K.D.K.), the National Science Foundation (NSF) (Grant CHE-9708222 to G.J.M.), and an NSF environmental research grant (CRAEMS, K.D.K. and G.J.M.). R.M.K. also acknowledges a Howard Hughes Summer Fellowship through the Johns Hopkins University.

Supporting Information Available: X-ray structure information (CIF files) for [(F$_8$TPP)Fe^{II}(CO)(THF)]·3THF (**1·3THF**) and [(F$_8$TPP)Fe^{II}(THF)$_2$]·2THF (**2·2THF**), UV−vis and ^{1,2}H/^{13}C NMR discussions (including Experimental Methods), and ^{13}C and ^{2}H NMR spectra for **1·3THF**. This material is available free of charge via the Internet at http://pubs.acs.org.

IC026307B